Toxicology and Applied Pharmacology 329 (2017) 334–346

Contents lists available at ScienceDirect

Toxicology and Applied Pharmacology

journal homepage: www.elsevier.com/locate/taap

Derivatives of alkyl gallate triphenylphosphonium exhibit antitumor activity in a syngeneic murine model of mammary adenocarcinoma

Liliana Peredo-Silva [a], Sebastián Fuentes-Retamal [a], Cristian Sandoval-Acuña [b], Mario Pavani [a], Juan D. Maya [a], Vicente Castro-Castillo [c], Matías Madrid-Rojas [d], Solange Rebolledo [d], Ulrike Kemmerling [e], Eduardo Parra [f], Jorge Ferreira [a,*]

[a] Clinical and Molecular Pharmacology Program, Institute of Biomedical Sciences (ICBM), Faculty of Medicine, University of Chile, Av. Independencia 1027, Santiago 8380453, Chile
[b] Institute of Biotechnology, Czech Academy of Sciences, Prúmyslová 595, Vestec, 25250, Prague, Czech Republic
[c] Department of Organic and Physical Chemistry, Faculty of Chemical and Pharmaceutical Sciences, University of Chile, Santos Dumont 964, Santiago 8380494, Chile
[d] Department of Chemistry, Faculty of Basic Sciences, Metropolitan University of Educational Sciences, Av. José Pedro Alessandri 774, Santiago 7760197, Chile
[e] Program of Anatomy and Developmental Biology, Institute of Biomedical Sciences (ICBM), Faculty of Medicine, University of Chile, Av. Independencia 1027, Santiago 8380453, Chile
[f] School of Medicine, Faculty of Health Sciences, University of Tarapacá, Av. General Velásquez 1775, Arica 1000007, Chile

ARTICLE INFO

Article history:
Received 16 January 2017
Revised 7 June 2017
Accepted 19 June 2017
Available online 21 June 2017

Keywords:
Alkyl gallate triphenylphosphonium derivatives
Syngeneic murine model of breast cancer
Uncoupling of mitochondrial function
Doxycycline
Delocalized lipophilic cation

ABSTRACT

We previously demonstrated that alkyl gallates coupled to triphenylphosphine have a selective and efficient antiproliferative effect by inducing mitochondrial uncoupling *in vitro* due to the increased mitochondrial transmembrane potential of tumor cells. Therefore, in this work, the *in vivo* antitumor activities of alkyl gallate triphenylphosphonium derivatives (TPP^+C_8, TPP^+C_{10} and TPP^+C_{12}) were evaluated in a syngeneic murine model of breast cancer. We found that TPP^+C_{10} increased the cytosolic ADP/ATP ratio and significantly increased the AMP levels in a concentration-dependent manner in TA3/Ha murine mammary adenocarcinoma cells. Interestingly, TPP^+C_{10} induced a decrease in the levels of cellular proliferation markers and promoted caspase-3 activation in tumor-bearing mice. Additionally, TPP^+C_{10} inhibited tumor growth in the syngeneic mouse model. Importantly, 30 days of intraperitoneal (i.p.) administration of the combination of TPP^+C_{10} (10 mg/kg/48 h) and the antibiotic doxycycline (10 mg/kg/24 h) completely eliminated the subcutaneous tumor burden in mice ($n = 6$), without any relapses at 60 days post-treatment. This enhancement of the individual activities of TPP^+C_{10} and doxycycline is due to the uncoupling of oxidative phosphorylation by TPP^+C_{10} and the inhibition of mitochondrial biogenesis by doxycycline, as demonstrated by loss of mitochondrial mass and overexpression of PGC1-α as an adaptive response. Moreover, i.p. administration of TPP^+C_{10} (10 mg/kg/24 h) to healthy mice did not produce toxicity or damage in organs important for drug metabolism and excretion, as indicated by hematological, biochemical and histological assessments. These findings suggest that the combination of TPP^+C_{10} with doxycycline is a valuable candidate therapy for breast cancer management.

1. Introduction

Gallic acid (GA; 3,4,5-trihydroxybenzoic acid) is a well-known polyphenol found abundantly in tea, grapes, berries and other fruits. GA has various biological activities, such as antibacterial, anti-melanogenic, antiviral and anti-inflammatory activities (Kang et al., 2008; Kratz et al., 2008; Yoon et al., 2013), in addition to its antineoplastic activity in various cancer cell types (Ji et al., 2009; Maurya et al., 2011), which merit attention in the development of drugs against cancer. GA and its alkyl derivatives, the propyl, octyl and lauryl gallates, have been widely

Abbreviations: $\Delta\Psi_m$, mitochondrial membrane potential; ADP, adenosine diphosphate; AMP, adenosine monophosphate; AP, alkaline phosphatase; AST, aspartate aminotransferase; ATP, adenosine triphosphate; BUN, blood urea nitrogen; CCCP, carbonyl cyanide *m*-chlorophenyl hydrazone; CK, creatine kinase; CK-MB, creatine kinase MB; DAB, diaminobenzidine; DMEM HG, Dulbecco's modified eagle medium-high glucose; DMSO, dimethyl sulfoxide; FITC, 4-fluorescein isothiocyanate; GA, gallic acid; HE, hematoxylin and eosin; HK-II, hexokinase 2; IIA, iodoacetate; IMM, inner mitochondrial membrane; LDH, lactate dehydrogenase; MCH, mean corpuscular hemoglobin; MCHC, mean corpuscular hemoglobin concentration; MCT, monocarboxylate transporter; MCV, mean corpuscular volume; OXPHOS, oxidative phosphorylation; PBS, phosphate-buffered saline; PCNA, proliferating cell nuclear antigen; PGC1-α, peroxisome proliferator-activated receptor-γ coactivator 1α; ROS, reactive oxygen species; TPP^+, triphenylphosphonium; TPP^+C_8, (8-((3,4,5-trihydroxybenzoyl)oxy)octyl) triphenylphosphonium; TPP^+C_{10}, (10-((3,4,5-trihydroxybenzoyl)oxy)decyl) triphenylphosphonium; TPP^+C_{12}, (12-((3,4,5-trihydroxybenzoyl)oxy)dodecyl) triphenylphosphonium; VDAC, voltage-dependent anion channel.

* Corresponding author.
E-mail address: jferreir@med.uchile.cl (J. Ferreira).

http://dx.doi.org/10.1016/j.taap.2017.06.017
0041-008X/

used as antioxidant additives in the food and pharmaceutical industries, and these compounds have demonstrated significantly low toxicities both *in vitro* and *in vivo* (Fiuza et al., 2004; Verma et al., 2013). Alkyl gallates have shown various biological activities, including cardiovascular protection, tyrosine kinase inhibition, and antibacterial, antifungal, anti-inflammatory, and anticancer activities, that in many cases are greater than those exhibited by GA itself (Locatelli et al., 2008, 2009). Additionally, it has been demonstrated that *n*-alkyl gallates can elicit the following effects: a) decrease mitochondrial membrane potential ($\Delta\Psi_m$); b) induce mitochondrial permeability transition pore opening; c) promote cytochrome *c* and apoptosis-inducing factor (AIF) release and procaspases and endonuclease G activation; and d) upregulate the expression of Bcl-2-associated X protein (BAX) and caspase-3, -4 and -9, subsequently causing DNA fragmentation (Yeh et al., 2011). It has also been reported that increasing concentrations of GA esters generate greater uncoupling of the oxidative phosphorylation (OXPHOS) system, as well as inhibit electron flow through the mitochondrial respiratory chain (at higher concentrations), mainly at NADH-CoQ oxidoreductase. These effects of GA esters prevent ATP synthesis and ultimately lead to cell death. Moreover, although the structure and lipophilicity of the alkyl side chain is important for the antitumor activity of these compounds, a "cutting" effect has been reported with increasing length of the alkyl chain of GA esters, leading to a decrease in their effects on a range of biological activities (Losada Barreiro et al., 2013).

Mitochondria play an important role in regulating energy metabolism, the cytosolic calcium concentration, ROS production and apoptosis. Importantly, mitochondria exhibit significant differences in OXPHOS between tumor and non-tumor cells; the inner mitochondrial membrane (IMM) of tumor cells has a $\Delta\Psi_m$ of approximately 150–180 mV, in which the potential is more negative on the matrix side, thus causing an increased $\Delta\Psi_m$. The $\Delta\Psi_m$ in tumor cells is much higher than the membrane potential of any other cell organelle and is higher than the $\Delta\Psi_m$ in other tissues and non-tumor cells (Modica-Napolitano and Singh, 2004). Furthermore, the activities of important enzymes involved in establishing the $\Delta\Psi_m$ are decreased in tumor cells (Lopez-Rios et al., 2007; Putignani et al., 2008), in association with a low respiration rate, which is possibly due to mitochondrial dysfunction (Modica-Napolitano and Singh, 2004); however, the latter point is under debate. In addition, tumor cells have increased expression of several proteins involved in glucose metabolism. In some cases, aerobic glycolysis may contribute >50% of total ATP synthesis and thus serve as the main source of energy in tumor cell (Pedersen, 2007). Nevertheless, many studies have confirmed the importance of OXPHOS in ATP production for tumor cells. This process enables direct delivery of newly synthesized ATP to hexokinase 2 (HK-II), an enzyme attached to the outer mitochondrial membrane through the voltage-dependent anion channel (VDAC) that is upregulated in tumor cells. Thus, HK-II uses the ATP synthetized *via* OXPHOS to phosphorylate and convert glucose into glucose-6-phosphate, one of the limiting steps in glycolysis (Rosano, 2011). This evidence suggests that mitochondria are excellent targets for antitumor therapies.

Because tumor cells have the highest $\Delta\Psi_m$, small molecules can be selectively targeted to tumor cell mitochondria (Coulter et al., 2000). To enhance the cytotoxic effect of GA esters, we synthesized delocalized lipophilic cations, in which GA with different alkyl chain lengths were conjugated to the triphenylphosphonium (TPP^+) moiety (Jara et al., 2014). These compounds, guided by the $\Delta\Psi_m$, selectively accumulate in tumor cells by binding directly to the phospholipid bilayer due to their large hydrophobic surface area. This interaction reduces the activation energy required to capture the TPP^+ group (Murphy and Smith, 2007), resulting in the accumulation of the target in the IMM at a nearly 500-fold higher concentration than that in the cytosol. We previously determined that alkyl gallate TPP^+ derivatives provoked mitochondrial uncoupling in mouse mammary adenocarcinoma cells (TA3/Ha), leading to a decrease in OXPHOS-mediated ATP synthesis and ultimately causing cell death (Jara et al., 2014). Also, we have tested the effectiveness of alkyl gallates in several human breast cancer cell lines, which differ in their expression of estrogen and epidermal growth factor receptors, as well as in their metabolic profile (Sandoval-Acuna et al., 2016). Because of these promising *in vitro* results, we evaluated the first *in vivo* antitumor activities of alkyl gallate-TPP^+ derivatives.

It is important to note that the "no observed adverse effect level" (NOAEL) of GA is approximately 120 mg/kg/day for rats and that the NOAEL of its alkyl gallate derivatives is approximately 1000 mg/kg/day in mice (van der Heijden et al., 1986; Lu et al., 2006). Furthermore, studies using phosphonium salts as contrast agents for diagnostic imaging (Kim et al., 2008) have elucidated two key points concerning these compounds: 1) they preferentially accumulate within tumor cells, and 2) the phosphonium cation itself does not impart cytotoxicity.

Because of the genetic complexity of cancer cells and the lack of a specific therapeutic target enabling personalized treatment, it is necessary to resort to an alternative therapy that focuses on a common trait of tumor cells. One of these features is the strict dependence on mitochondrial biogenesis for the anchorage-independent clonal expansion and survival of cancer stem cell populations. Considering this dependence, many classes of FDA-approved antibiotics inhibit mitochondrial biogenesis or OXPHOS as a mild side effect, and their ability to eradicate cancer stem cells has been studied (Lamb et al., 2015). Among these drugs, doxycycline represents an attractive new anticancer agent. Doxycycline is a broad-spectrum antibiotic of the tetracycline class that inhibits protein synthesis by preventing the binding of activated aminoacyl-tRNAs to the A site of the 30S subunit of bacterial ribosomes. Importantly, the 30S subunit of the bacterial ribosome is homologous to the 28S subunit of the mitochondrial ribosome; as a consequence, tetracycline-based antibiotics inhibit mitochondrial biogenesis. Moreover, doxycycline has been used in human tumor xenograft and other animal models to significantly reduce the tumor burden and even suppress metastatic cancer cell growth (Duivenvoorden et al., 2002; Shen et al., 2010; Chang et al., 2014).

Importantly, combination therapies are known to be more clinically effective than individual therapies against cancer. Thus, based on the properties of alkyl gallate TPP^+ derivatives described above and the evidence of their cytotoxicity *in vitro*, we investigated the antitumor effects of these compounds (chemical structures in Supplementary Fig. 1) in a syngeneic murine model. In addition, according to the results from studies of doxycycline in different animal models of breast cancer (Lamb et al., 2015), the effect of the combination of TPP^+C_{10} and doxycycline on mitochondrial biogenesis and the capacity of this combination to reduce tumor growth were analyzed. The results revealed that this combined treatment decreased the mitochondrial mass and consequently increased the levels of peroxisome proliferator-activated receptor-γ coactivator 1α (PGC1-α), the master regulator of mitochondrial biogenesis, as compensatory effect. Moreover, combined doxycycline and TPP^+C_{10} treatment completely eliminated the tumor burden *in vivo*, without recurrence at 60 days post-treatment. This combination treatment might be a beneficial therapeutic strategy for the management of breast cancer.

2. Materials and methods

2.1. Drugs used in this study

The compounds used in the present study were synthesized according to Jara et al. (2014) and were numbered based on the size of the carbon chain:

TPP^+C_8: triphenyl (8-((3,4,5-trihydroxybenzoyl)oxy)octyl) phosphonium bromide;
TPP^+C_{10}: triphenyl (10-((3,4,5-trihydroxybenzoyl)oxy)decyl) phosphonium bromide; and
TPP^+C_{12}: triphenyl (12-((3,4,5-trihydroxybenzoyl)oxy)dodecyl) phosphonium bromide.

2.2. TA3/Ha cell line

TA3/Ha cells were kindly provided by Dr. Gasic, University of Pennsylvania, and have been used by our laboratory since 1989. This cell lines were propagated until the day of the assay by weekly intraperitoneal (i.p.) inoculation of ascitic fluid into young adult male AJ mice and harvested after 5–7 days (a description of selected features of this tumor cell line is provided in the Supplementary information), however no authentication has been performed.

2.3. Determination of O_2 consumption and H^+ extrusion

Oxygen consumption by TA3/Ha mouse mammary adenocarcinoma cells was measured polarographically using a Clark electrode (Yellow Spring Instruments Co.), and the release of H^+ was measured potentiometrically using a pH electrode (Cole-Palmer) as described in the Supplementary information. Analysis of the recorded data was performed using SigmaPlot 12 (Systat Software, Inc., San Jose, CA). For this experiment, TA3/Ha cells were obtained directly from mouse as ascitic tumor, and were prepared as follows: TA3/Ha cells were resuspended in medium consisted in 150 mM NaCl, 5 mM KCl and 1 mM Tris-HCl, pH 7.0. As respiratory substrate glutamine 5 mM and glucose 5 mM were used. The compounds added in each measurement are indicated in the traces.

The calibration of H^+ release was determined by backtitration with known amounts of 0.1 M HCl. The solubility of oxygen in the air-saturated test medium used was determined to be 452.5 ng atoms of oxygen/mL at 25 °C.

2.4. Analysis of the colocalization of C_{12}-FITC and TPP^+C_{12}-FITC with mitochondria in TA3/Ha cells

For visualization, TPP^+C_{12} was conjugated to the fluorescent compound fluorescein isothiocyanate-4 (FITC) as described by Han et al. (2008). Detailed methodology is provided in the Supplementary information. For quantification of colocalization of MitoTracker-orange MTO (mitochondria) with FITC conjugated to lauryl gallate (C_{12}-FITC) or a gallic acid derivative (TPP^+C_{12}-FITC), colocalization ratios were calculated based on effective colocalization using local Manders overlap coefficients.

2.5. Determination of the ADP/ATP ratio and AMP levels in TA3/Ha cells

The ADP/ATP ratio was calculated using an ADP/ATP ratio assay (Bioluminescent) Kit (Abcam®, ab65313) according to the manufacturer's instructions. AMP levels were measured using an AMP-Glo™ Assay kit (Promega® V5011) according to the manufacturer's instructions; detailed methodology is provided in the Supplementary information. Values are expressed as the ATP/ADP ratio or in relative luminescence units.

2.6. Syngeneic mouse model and experimental procedure

Adult AJ male mice, weighing between 28 and 30 g, were purchased from the animal facility of the Faculty of Medicine of the University of Chile. The animals were housed in a stable laboratory environment with a 12 h light/dark cycle at 21 °C in accordance with institutional animal protocols (University of Chile Committee on Animal Welfare). Detailed methodology of the propagation of the TA3/Ha cell line in animals for production of the syngeneic murine model is provided in the Supplementary information.

Prior to injection, TA3/Ha cells were washed with 0.9% NaCl and centrifuged at 3000 rpm for 5 min; the cell pellets were suspended in 100 μL of 0.9% NaCl and injected (1×10^6 cells/mouse) subcutaneously into the back of the mice. The animals were randomly allocated to the different treatment groups ($n = 6$). Detailed methodology is provided in the Supplementary information.

2.7. Hematology, biochemical analysis and cardiac enzyme activity evaluation

Groups of six mice were i.p. administered 10 or 50 mg/kg/48 h of a tested compound or vehicle for 30 days. At the end of treatment, a fresh blood sample was collected prior to anesthesia with ketamine/xylazine (100/5 mg/kg) and transferred into a Microtainer tube containing EDTA for hematological evaluation or into a Microtainer tube containing separating gel for biochemical analysis and cardiac enzyme activity evaluation; for details on the parameters evaluated, see the Supplementary information. The analyses of these parameters were performed in the Clinical Laboratory of the Clinical Hospital of the University of Chile.

2.8. Immunofluorescence analysis of the cellular proliferation markers Ki-67 and PCNA

Animals were treated i.p. with 10 mg/kg/48 h of a tested compound or vehicle for 28 days. At the end of treatment, the surviving mice were sacrificed, and their tumor tissue was removed. The samples were processed for conventional immunofluorescence. Detailed methodology is provided in the Supplementary information.

2.9. Immunohistochemistry for caspase 3, caspase 9 and translocase of outer mitochondrial membrane-20 (TOMM-20)

Animals were treated i.p. with 10 mg/kg/48 h of a tested compound or vehicle for 28 days. At the end of treatment, the surviving mice were sacrificed, and their tumor tissue was removed. The samples were processed for conventional immunohistochemistry. Detailed methodology is provided in the Supplementary information.

2.10. Western blotting for active caspase-3, active caspase-9 and PGC1-α

Western blotting analysis for active caspase-9 was performed in TA3/Ha cells. These cells were treated for 6 h with different concentrations of TPP^+C_{10}; for detailed methodology, see the Supplementary information. For Western blotting for PGC1-α, TA3/Ha cells were treated for 24 h with different concentrations of doxycycline, TPP^+C_{10} or doxycycline together with TPP^+C_{10} (as detailed in the Supplementary information). For determination of caspase-3 and procaspase-9 expression by Western blotting in tumor tissue, animals were treated i.p. with 10 mg/kg/48 h of a tested compound or vehicle during 28 days. At the end of treatment, protein expression in tumor tissue was measured *via* SDS-PAGE; for detailed methodology, see the Supplementary information. Immunoreactive bands were quantified using ImageJ 1.47v software.

2.11. Flow cytometric analysis of mitochondrial mass and active caspase-3 in TA3/Ha cells

To measure mitochondrial mass, TA3/Ha cells were treated with different concentrations of doxycycline and/or TPP^+C_{10} and then stained with MitoTracker® Green FM (#M7514 Invitrogen; λ_{ex} 490/λ_{em} 516), a mitochondrial stain that localizes to mitochondria regardless of $\Delta\Psi_m$; detailed methodology is provided in the Supplementary information.

For active caspase-3, TA3/Ha cells were treated with different concentrations of TPP^+C_{10} for 24 h and then processed using PE Active Caspase-3 Apoptosis Kit (BD Bioscience®, #550914) according to the manufacturer's instructions, see the Supplementary information.

2.12. Statistical analysis

Survival of animals was statistically analyzed using the Kaplan-Meier method. One-way or two-way ANOVA (followed by Bonferroni

post hoc analysis) was performed as appropriate. For all experiments, statistical significance was set at $p < 0.05$. Analyses were performed using GraphPad Prism Version 5.00 statistical software.

3. Results

3.1. Metabolic characterization of mouse mammary adenocarcinoma TA3/Ha cells: oxygen uptake and proton extrusion

The kinetics of oxygen uptake and extracellular acidification in TA3/Ha tumor cells were measured. Such processes, measured as oxygen consumption and H^+ extrusion, were at maximal rates when adding cells because all electron carriers of the respiratory chain were completely reduced (anaerobic conditions) and the suspension medium was slightly acidic.

Representative traces of oxygen consumption and H^+ extrusion in the presence of only endogenous substrates (Fig. 1A) showed a decrease in the dissolved oxygen concentration with apparent-first order kinetics, along with a slight linear increase in H^+ extrusion. Addition of glutamine (Fig. 1B) induced a more rapid linear decrease in the oxygen concentration, as well as a corresponding increase in H^+ extrusion. Interestingly, under total anaerobic conditions, a very slight linear increase in H^+ release was observed. When only glucose was added (Fig. 1C), the rate of oxygen consumption was very similar to that shown in Fig. 1B, but the linear rate of H^+ release was surprisingly increased, even under aerobic conditions. When glutamine and glucose were simultaneously added (Fig. 1D), the rate of oxygen consumption was very similar to that shown in Fig. 1C. However, a slower linear increase in H^+ extrusion was observed, although this rate was significantly increased under anaerobic conditions. When glutamine and glucose were added together with the Complex I inhibitor rotenone (Fig. 1E), or the Complex III inhibitor Antimycin A (Fig. 1F), an abrupt and nearly complete inhibition of oxygen consumption was observed under both conditions, accompanied by an immediate increase in the rate of H^+ release. Similarly, in cells respiring in the presence of glutamine, glucose, and the ATP synthase inhibitor oligomycin, the oxygen consumption rate was reduced, and the H^+ release rate was abruptly increased. Upon the addition of the uncoupler CCCP or TPP^+C_{10}, a sudden increase in the oxygen consumption rate occurs with a reduced H^+ extrusion (Fig. 1G–H). The same behavior was observed when using another classic uncoupler, 2,4-DNP (Supplementary Fig. 2). Interestingly, the H^+ release rate decreased when all oxygen was exhausted. In the presence of the glycolysis inhibitor iodoacetate (IIA), the oxygen consumption rate was not affected, but the H^+-release rate was strongly reduced (Fig. 1I). When oligomycin was also added, this rate slightly decreased, attaining a similar slope as the CCCP-added cells, reaching almost zero when all the oxygen was exhausted.

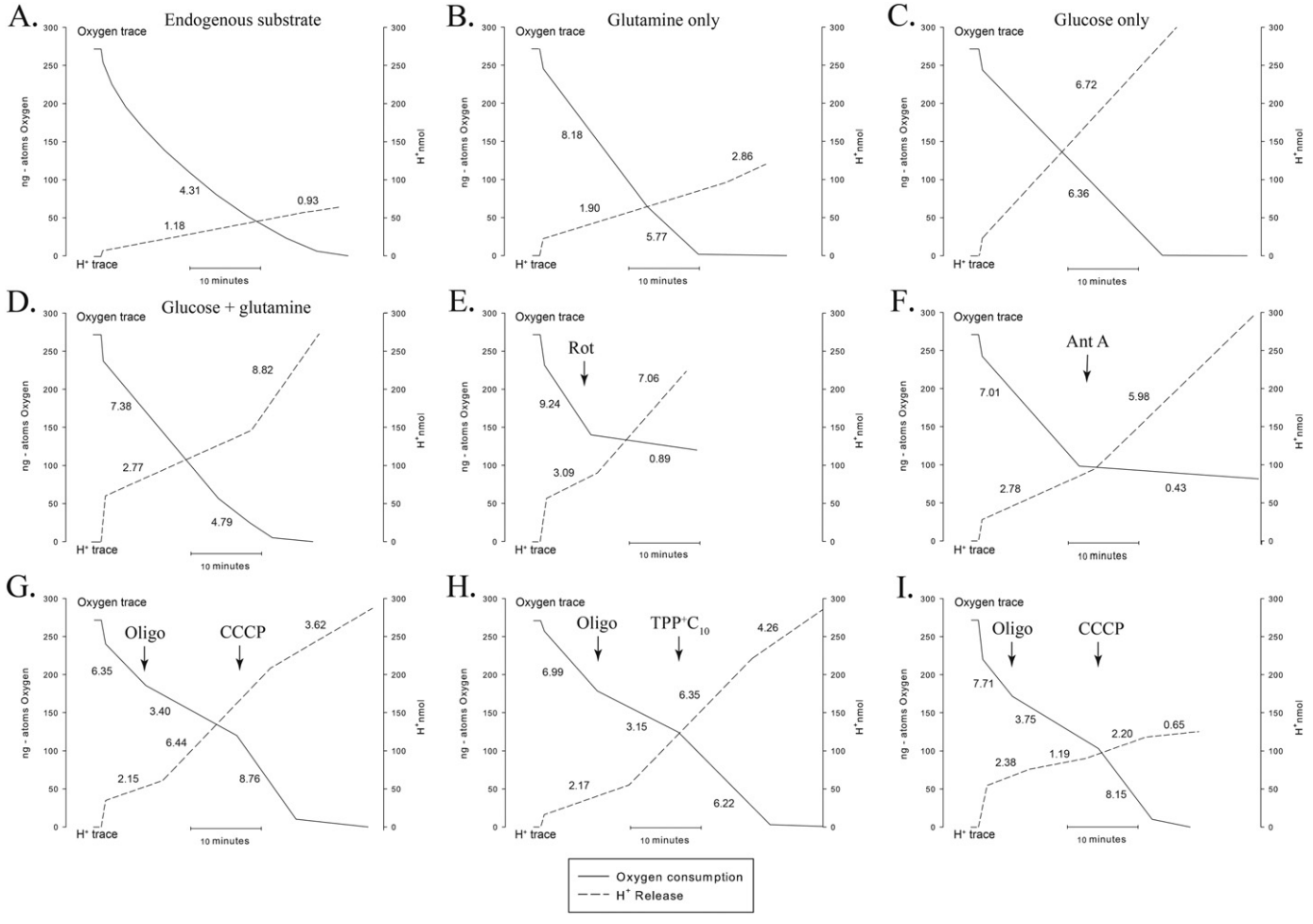

Fig. 1. Metabolic characterization of TA3/Ha cells. Representative traces of oxygen consumption and H^+ release in the presence of A. endogenous substrate, B. 5 mM glutamine, C. 5 mM glucose, D. 5 mM glutamine and 5 mM glucose, E. the Complex I inhibitor rotenone (4 μM) together with glutamine and glucose as substrates, F. the Complex III inhibitor Antimycin A (1.25 ng/mL) together with glutamine and glucose as substrates, G. 1.5 μg/mL oligomycin and the uncoupler CCCP (50 nM) in the presence of glutamine and glucose as substrates, H. oligomycin and TPP^+C_{10} (10 μM) in the presence of glutamine and glucose as substrates, and I. oligomycin and CCCP in the presence of glutamine and glucose as substrates as well as the glycolysis inhibitor IIA (1 mM). The number below the solid trace represents ng-atoms O/min·mg protein, and the number above the dotted trace represents nmol H^+/min·mg protein. The lines were fitted using SigmaPlot 12 software, and the slopes were calculated using Excel. Rot: Rotenone; Ant A: Antimycin A; Oligo: Oligomycin.

3.2. Alkyl gallate triphenylphosphonium derivatives colocalize with tumor cell mitochondria and increase the ADP/ATP ratio and AMP levels in TA3/Ha cells

To evaluate the influence of the TPP^+ moiety on the degree of mitochondrial tropism of alkyl gallate derivatives in TA3/Ha cells, we evaluated the percentage of colocalization of lauryl gallate-TPP^+ (TPP^+C_{12}) relative to lauryl gallate alone. The results showed that lauryl gallate-FITC was widely distributed in the cytosol of tumor cells, showing only 33% colocalization with mitochondria (Fig. 2Ad). In contrast, TPP^+C_{12}-FITC showed a high level of colocalization with mitochondria (76%) in TA3/Ha cells (Fig. 2Ah). These results indicate the importance of TPP^+ to the selective guidance of a pharmacophore to tumor cell mitochondria driven by the more negative charge of the mitochondrial matrix in tumor cells.

The derivative TPP^+C_{10} was established as a safe mitochondrial uncoupling agent based on its concentration-dependent activity, which showed a therapeutic range of approximately 500-fold (Jara et al., 2014). Moreover, it was expected that this effect would be accompanied by a decrease in intracellular ATP content. Therefore, the ADP/ATP ratio and AMP levels were measured. Treatment with TPP^+C_{10} increased the ADP/ATP ratio in a concentration-dependent manner (Fig. 2B). Additionally, AMP levels were increased greatly in the presence of TPP^+C_{10} (Fig. 2C), indicating that the compensatory mechanism for maintaining ATP levels (adenylate kinase activity) provoked an increase in AMP levels. This result is directly related to the metabolic stress caused by the uncoupling activity of TPP^+C_{10}, which could lead to cell death.

3.3. Alkyl gallate triphenylphosphonium derivatives did not cause systemic toxicity or damage to organs important for drug metabolism and excretion

To assess the possible systemic toxicity of the tested compounds, hematological and biochemical parameters were analyzed. Because of the mitochondrial tropism of the tested compounds, cardiac damage might be expected; thus, changes in cardiac enzyme activity levels were assessed. Additionally, the survival of animals at different doses of the tested compounds was evaluated, and it was determined that i.p. administration of 10 mg/kg/48 h of all compounds for 30 days led to

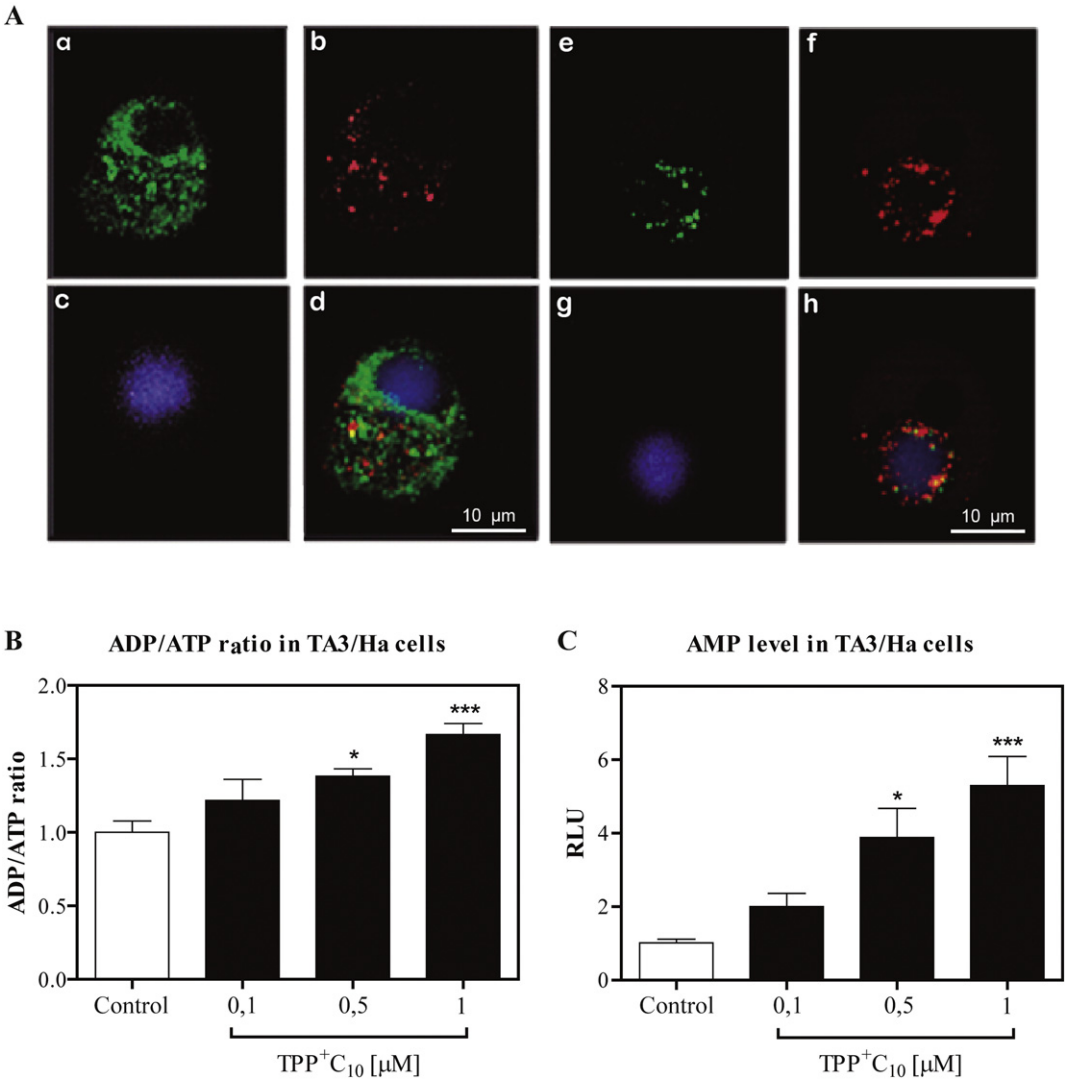

Fig. 2. Colocalization of TPP^+C_{10} with mitochondria and the effect of TPP^+C_{10} treatment on the ADP/ATP ratio and AMP levels in mitochondria of TA3/Ha cells. A. The graphs show representatives images of at least three independent experiments: a. C_{12}-FITC (lauryl gallate conjugated to FITC); b. MTO (MitoTracker orange); c. DAPI; d. merge; e. TPP^+C_{12}-FITC; f. MTO (MitoTracker orange); g. DAPI; and h. merge. The Manders overlap coefficient (R) was 0.33 for the experiment shown in d. The Manders overlap coefficient (R) was 0.76 for the experiment shown in h. Scale bar: 10 μm. B. ADP/ATP ratio; the graph shows the means ± SD of at least three independent experiments C. AMP levels; the graph shows the means ± SD of at least three independent experiments in relative luminescence units. 1.0×10^5 TA3/Ha cells/mL were incubated for 2 h with 0.1, 0.5 or 1 μM TPP^+C_{10}. Then, the ADP/ATP ratio and AMP levels were calculated as described in the Methods. Error bars represent 95% CI. One-way ANOVA followed by the Bonferroni post-test. $^*p < 0.05$ and $^{***}p < 0.001$ indicate statistically significant differences compared with the control group.

86% survival. Moreover, at this dose, no loss of body weight (Supplementary Fig. 3), ruffling of fur, or alteration in behavior was detected.

Treatment with TPP^+C_{10} or TPP^+C_{12} at 10 or 50 mg/kg did not alter hematological parameters (Table 1A). Similarly, treatment with these compounds at 10 mg/kg did not alter biochemical parameters. Only in mice treated with TPP^+C_{12} at 50 mg/kg, there was an increase in the levels of blood urea nitrogen (BUN) and aspartate aminotransferase (AST) (indicators of renal and hepatic dysfunction, respectively) (Table 1B). However, at 10 mg/kg TPP^+C_{12}, there was no change in the parameters measured. Moreover, there was no increase in cardiac enzyme activity levels for any of the compounds assessed (Table 1B). To further confirm the safety of these compounds, histopathological analysis of cardiac, hepatic and renal tissue was conducted, and the results were consistent with those of hematological analysis. At 10 mg/kg, no morphological changes in organs or fibrosis in cardiac tissue were detected (Supplementary Fig. 4). Altogether, these results confirmed that i.p. administration of 10 mg/kg (TPP^+C_{10} or TPP^+C_{12}) is safe, as these treatments did not cause systemic toxicity or damage to the organs responsible for the metabolism and excretion of these compounds.

3.4. TPP^+C_{10} enhanced the inhibition of mitochondrial biogenesis induced by doxycycline

It has been widely established that doxycycline can inhibit mitochondrial protein synthesis as a side effect and can therefore inhibit mitochondrial biogenesis. Thus, this antibiotic has the ability to inhibit the anchorage-dependent survival and spread of cancer stem cells as well as the formation of metastases in animal models of cancer. Furthermore, as described for the above analysis, TPP^+C_{10} can alter mitochondrial function by uncoupling OXPHOS. For this reason, the effect of the combination of doxycycline and TPP^+C_{10} on mitochondrial biogenesis was analyzed.

This combined treatment decreased the mitochondrial mass of TA3/Ha cells, as assessed by MitoTracker Green staining based on FACS (Fig. 3A–B). This decrease was statistically significant for 50, 100 and 200 μM doxycycline compared to the control treatment. More importantly, the combination of 1.0 μM TPP^+C_{10} and 25 or 200 μM doxycycline further decreased the mitochondrial mass compared with 25 or 200 μM doxycycline alone (Fig. 3B). Moreover, combined treatment of 1.0 μM

Table 1
(A) Hematologic parameters and (B) Biochemical parameters of healthy mice treated with TPP^+C_{10} or TPP^+C_{12}.

Parameter	Control	TPP^+C_{10}	TPP^+C_{10}	TPP^+C_{12}	TPP^+C_{12}
		10 mg/kg	50 mg/kg	10 mg/kg	50 mg/kg
(A) Hematologic parameters					
Red blood cell count 10^6 cells/mm^3	8.5 ± 0.3	7.9 ± 0.7	8.2 ± 0.6	7.87 ± 0.6	8.3 ± 0.5
Packed cell volume %	49.9 ± 0.7	46.2 ± 3.1	45.1 ± 4.7	45.9 ± 1.1	46.6 ± 0.8
Hemoglobin level g/dL	12.7 ± 0.4	12.2 ± 0.8	13.4 ± 1.1	12.5 ± 0.3	12.1 ± 0.1
MCV fL	58.5 ± 1.3	58.4 ± 3.6	54.8 ± 5.9	58.6 ± 6.1	56.4 ± 2.9
MCH pg	14.9 ± 0.9	15.5 ± 0.4	16.3 ± 0.5	15.9 ± 0.9	14.7 ± 1.1
MCHC g/dL	25.5 ± 0.9	26.5 ± 1.3	29.9 ± 2.7	25.9 ± 0.5	26.0 ± 0.7
White blood cell count 10^3 cells/μL	12.3 ± 8.9	5.9 ± 1.6	6.8 ± 1.6	4.3 ± 2.2	5.42 ± 0.8
Monocyte count 10^3 cells/μL	6.7 ± 1.5	8.3 ± 1.2	12.0 ± 4.1	12.5 ± 0.7	7.7 ± 0.9
Lymphocyte count 10^3 cells/μL	62.7 ± 6.0	62.7 ± 13.1	53.5 ± 9.1	56.0 ± 5.7	47.3 ± 8.8
Platelet count 10^3 platelets/μL	1066 ± 157	1047 ± 266	806.5 ± 235	1037 ± 111	1410 ± 86
(B) Biochemical parameters					
Glucose mg/dL	205.3 ± 22.1	196 ± 38.8	182 ± 14.5	208 ± 13.4	172 ± 33.9
Total protein g/dL	5.0 ± 0.1	4.65 ± 0.07	4.8 ± 0.7	5.0 ± 0.2	4.5 ± 0.2
Uric acid mg/dL	1.1 ± 0.1	1.3 ± 0.2	1.3 ± 0.6	1.5 ± 0.4	1.1 ± 0.2
Albumin g/dL	2.0 ± 0.2	1.9 ± 0.07	1.9 ± 0.1	2.1 ± 0.1	1.8 ± 0.1
Cholesterol mg/dL	120 ± 15.8	94.5 ± 10.6	116 ± 9.5	115 ± 18.3	89 ± 7.1
Blood urea nitrogen (BUN) mg/dL	19 ± 1.7	21.5 ± 2.1	25 ± 1.3	18 ± 0.5	39.5 ± 2.1*
Total bilirubin mg/dL	0.23 ± 0.05	0.15 ± 0.1	0.2 ± 0.04	0.35 ± 0.07	0.23 ± 0.1
Aspartate aminotransferase (AST) U/L	161 ± 50.3	155 ± 28.3	172 ± 12.2	194 ± 8.5	606 ± 36.7*
Alkaline phosphatase U/L	231 ± 35.3	171 ± 80.6	182 ± 21.4	238 ± 12.7	161 ± 14.8
Lactic dehydrogenase (LDH) U/L	9235 ± 257	9143 ± 900	–	9965 ± 262	–
CK U/L	387 ± 41.8	270 ± 77.7	288 ± 44.5	276 ± 61.1	327 ± 81.3
CK-MB U/L	633 ± 44.5	434 ± 49.9	–	400 ± 97.7	–

Animals were treated with 10 or 50 mg/kg body weight TPP^+C_{10} or TPP^+C_{12} every 48 h. Values are presented as means ± SD of two independent experiments ($n = 6$ mice per group). One-way ANOVA. *$p < 0.05$ indicates a statistically significant difference compared with the control group.

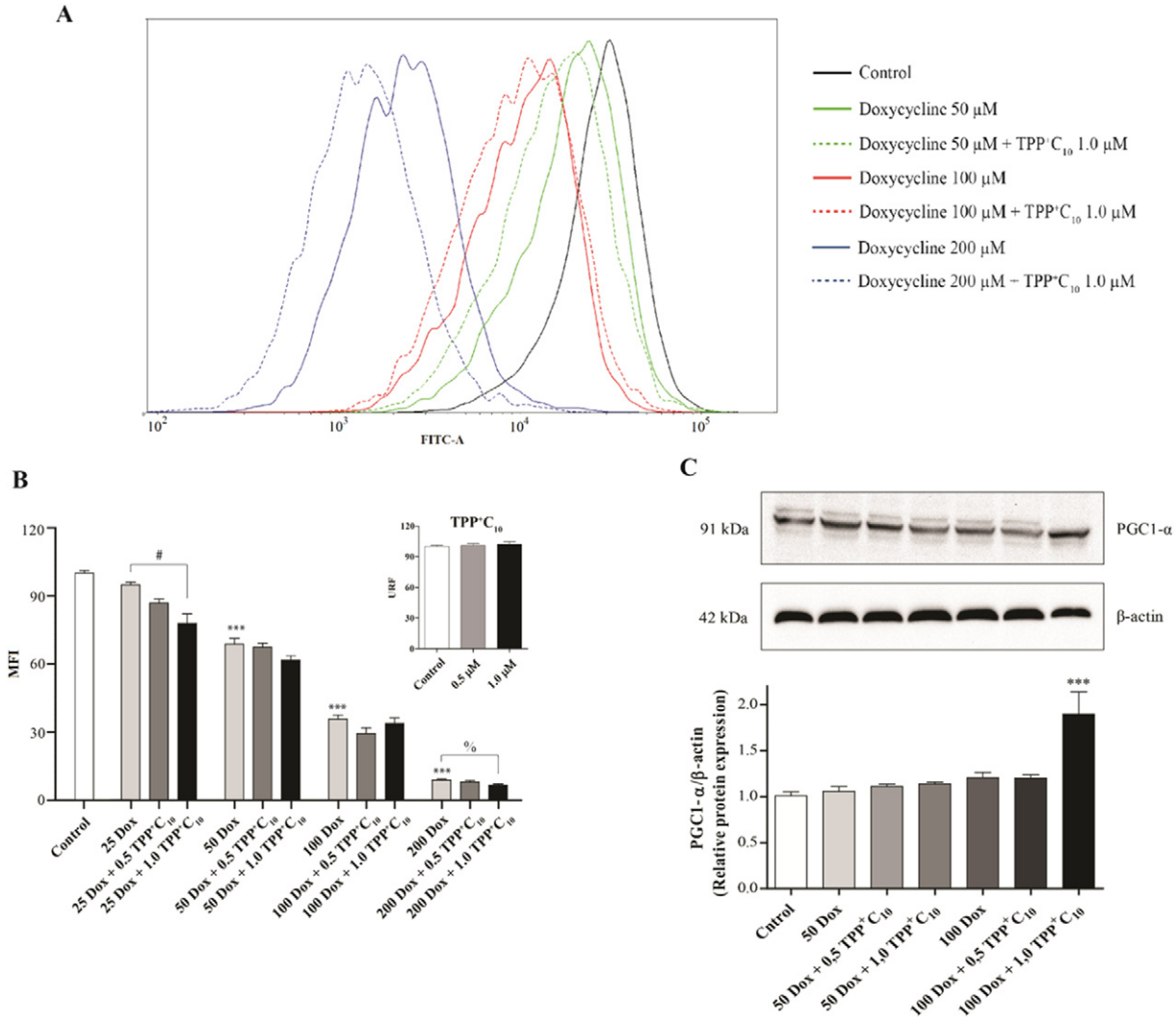

Fig. 3. TPP^+C_{10} enhanced the inhibition of mitochondrial biogenesis induced by doxycycline. TA3/Ha cells were treated with increasing concentrations of TPP^+C_{10} and doxycycline for 24 h as described in the Methods. A. Representative histograms of flow cytometry using MitoTracker® Green FM. B. Representative mean fluorescence intensity (MFI) from three independent experiments. C. Western blotting for PGC1-α from four independent experiments. One-way ANOVA followed by the Bonferroni post-test. ***$p < 0.001$ indicates a statistically significant difference compared with the control group. #: 25 Dox statistically significantly different compared with 25 Dox + 1.0 TPP^+C_{10}. %: 200 Dox statistically significantly different compared with 200 Dox + 1.0 TPP^+C_{10}.

TPP^+C_{10} and 100 μM doxycycline increased the protein expression of PGC1-α, as assessed by Western blotting (Fig. 3C). PGC1-α is considered a key regulator of mitochondrial biogenesis and is required for the transcription of nuclear-encoded mitochondrial genes, which triggers mitochondrial biogenesis. The observed effect of the combination treatment on this transcription coactivator may be due to an adaptive response of the tumor cells to maintain their survival and growth, upregulating PGC1-α to offset the loss of mitochondrial function. Together, these results established that combination treatment of TPP^+C_{10} and doxycycline increased the deleterious effects on mitochondrial function in TA3/Ha cells, suggesting that this treatment may be an important alternative cancer therapy that warrants investigation *in vivo*.

3.5. Alkyl gallate triphenylphosphonium derivatives decreased the expression of cell proliferation markers, caused caspase-dependent cell death and reduced mitochondrial biomass in vivo

To evaluate the effect of the combination treatment on cell proliferation, the expression of two proliferation markers widely used in the clinic was assessed. Ki-67 expression correlates with disease prognosis, tumor stage and the treatment response, while PCNA is a nuclear protein that is detected in the early G1 phase of the cell cycle, with a peak of expression in the S phase. Treatment with TPP^+C_{10} or TPP^+C_{12} significantly decreased the number of Ki-67-positive cells (Fig. 4A), although this reduction was more pronounced for TPP^+C_{10} (by 43% and 59%, respectively). Treatment with either TPP^+C_{10} or TPP^+C_{12} induced a decrease in the levels of the marker PCNA, but this decrease was significant only for TPP^+C_{10} (Fig. 4B).

Through *in vitro* analysis in TA3/Ha cells, the activation of caspase-9 (after 6 h of stimulation) and caspase-3 (after 24 h of stimulation) induced by TPP^+C_{10} was evaluated. A concentration-dependent increase of active caspase-3 (Fig. 5A) as well as active caspase-9 (Fig. 5B) was clearly observed. These results were corroborated *in vivo*. TPP^+C_{10} produced significant activation of caspase-3 in tumor tissue, and TPP^+C_{12} produced a trend towards an increase in the expression of this enzyme. Induction of apoptosis by TPP^+C_{10} in tumor tissue was confirmed by TUNEL positive signal (Supplementary Fig. 5). In contrast, no alteration in procaspase-9 expression was observed after either treatment (Fig. 5C–E).

The distribution of mitochondrial mass was assessed by measuring the expression of TOMM-20, established as a marker of mitochondrial mass and biogenesis. TPP^+C_{10}, but not TPP^+C_{12}, significantly decreased TOMM-20 expression in tumor tissue (Fig. 6). Altogether, these results indicate that i.p. administration of 10 mg/kg TPP^+C_{10} causes a strong

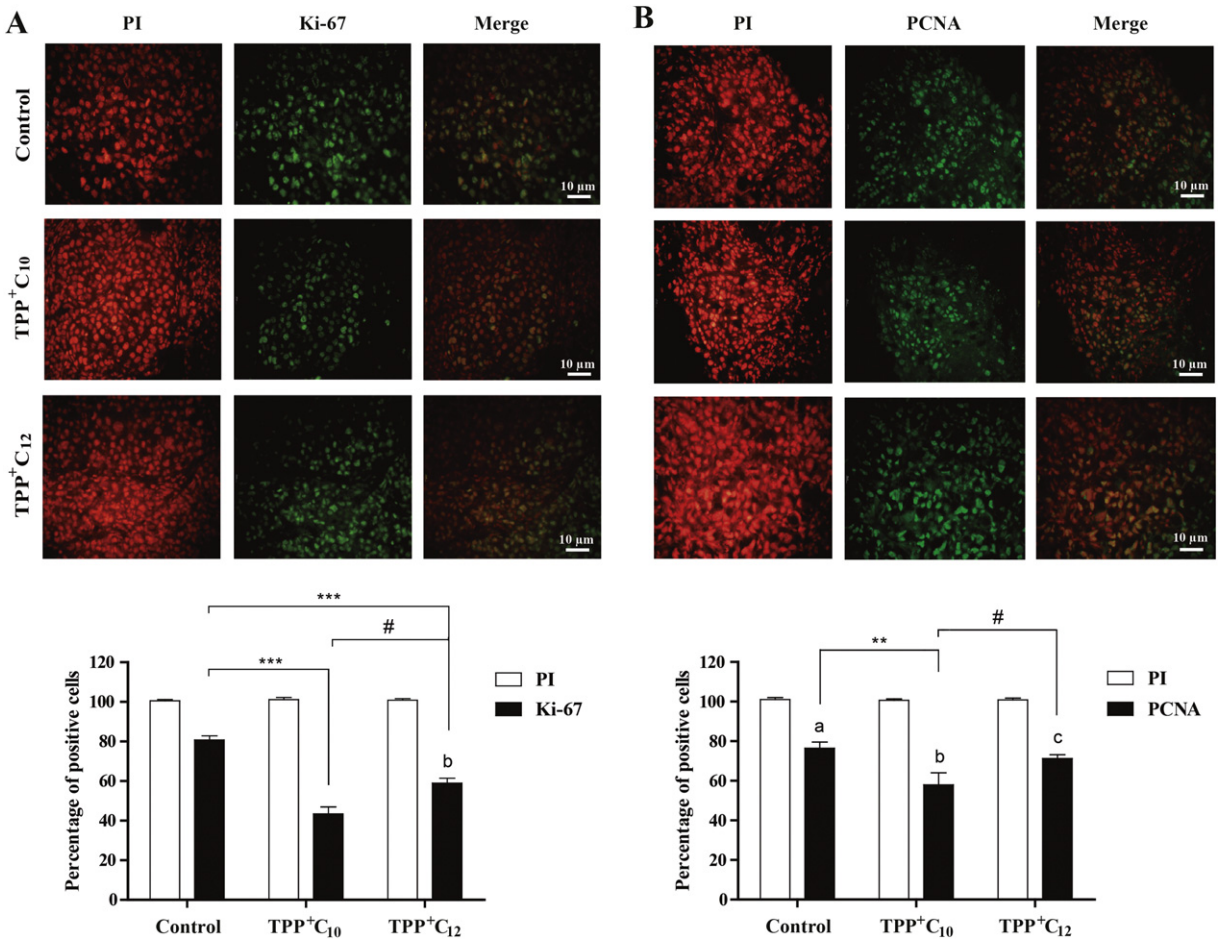

Fig. 4. Effect of TPP^+C_{10} and TPP^+C_{12} on the expression of the proliferation markers Ki-67 and PCNA in tumor tissue. Mice were treated with 10 mg/kg body weight of each compound or vehicle as appropriate every 48 h for a period of 30 days. A. Representative images of immunofluorescence for Ki-67 and B. for PCNA. Graphs show quantification of three independent experiments for each marker. Two-way ANOVA followed by the Bonferroni post-test for immunofluorescence quantification. $^{**}p < 0.01$, and $^{***}p < 0.001$ indicate statistically significant differences compared to the control group. a, b, and c indicate statistically significant differences compared to PI-stained tissue. $^{\#}$Statistically significant difference between treatments (TPP^+C_{10} *vs.* TPP^+C_{12}). PI: Propidium Iodide. Scale bar: 10 µm.

response in animals treated with a factor benefiting prognosis by activating the apoptotic cell death pathway *in vivo*. Additionally, TPP^+C_{10} appeared to induce a decrease in mitochondrial biomass in tumor-bearing mice.

3.6. Treatment with alkyl gallate triphenylphosphonium derivatives prevents tumor growth and the combination of TPP^+C_{10} and doxycycline completely eradicates the tumor burden

Using a syngeneic murine model, we examined the effect of the tested compounds on tumor growth. Treatment with 10 mg/kg TPP^+C_{10} produced a significant reduction in tumor growth (Fig. 7A–C), leading to a survival rate of 70% at 40 days post-inoculation (Fig. 7B). Conversely, TPP^+C_{12} produced a non-significant decrease in tumor growth, and the TPP^+C_8 showed the same tumor size as the control group at 28 days of treatment (Fig. 7A). In conclusion, TPP^+C_{10} is the most effective compound in decreasing tumor growth, promoting a high survival rate of the tumor bearing-mice.

Furthermore, we evaluated the ability of TPP^+C_{10} in combination with doxycycline to inhibit tumor growth. Although the treatment with doxycycline alone did not cause a significant reduction in tumor growth, the combination of TPP^+C_{10} and doxycycline eliminated 97.05% of the tumor burden at 30 days post-treatment (Fig. 7D). Importantly, after 60 days post-treatment, the combination treatment group maintained 100% survival, whereas the animals in the control group did not survive for the entire treatment period (Fig. 7F). Moreover, at 60 days after the combined treatment, recurrence of tumor growth was not observed, showing the excellent efficacy of this combination. Additionally, treatment with TPP^+C_{10} and doxycycline produced no systemic toxicity.

4. Discussion

The tumor microenvironment, especially that of solid tumors, is characterized by low contents of oxygen (regions of hypoxia and anoxia) and nutrients, mainly due to deficiencies in the tumor vasculature (Spill et al., 2016). As a result, oxygen becomes highly scarce. Survival of tumor cells under these hostile conditions requires the development of adaptive strategies to more efficiently manage the defective oxygen supply by favoring metabolic pathways that could be less efficient. Oxygen is reserved for vital activities, such as its contribution of mitochondrial ATP *via* HK-II activity and the maintenance of the mitochondrial calcium-buffering system. Therefore, tumor cells are able to change their preferences for one metabolic pathway with another, indicating this feature as sign of cell transformation.

Glucose metabolism in tumor tissue is upregulated compared to that in normal tissue, even in a normoxic environment (Warburg effect). However, a contribution of OXPHOS to tumor cell bioenergetics and metabolism has not been ruled out. Due to their high proliferative rate, cancer cells have a high demand for hydrocarbon and nitrogen compounds to increase their biomass, promote cell migration and metastasis formation, and maintain high levels of NAD(P)H for different

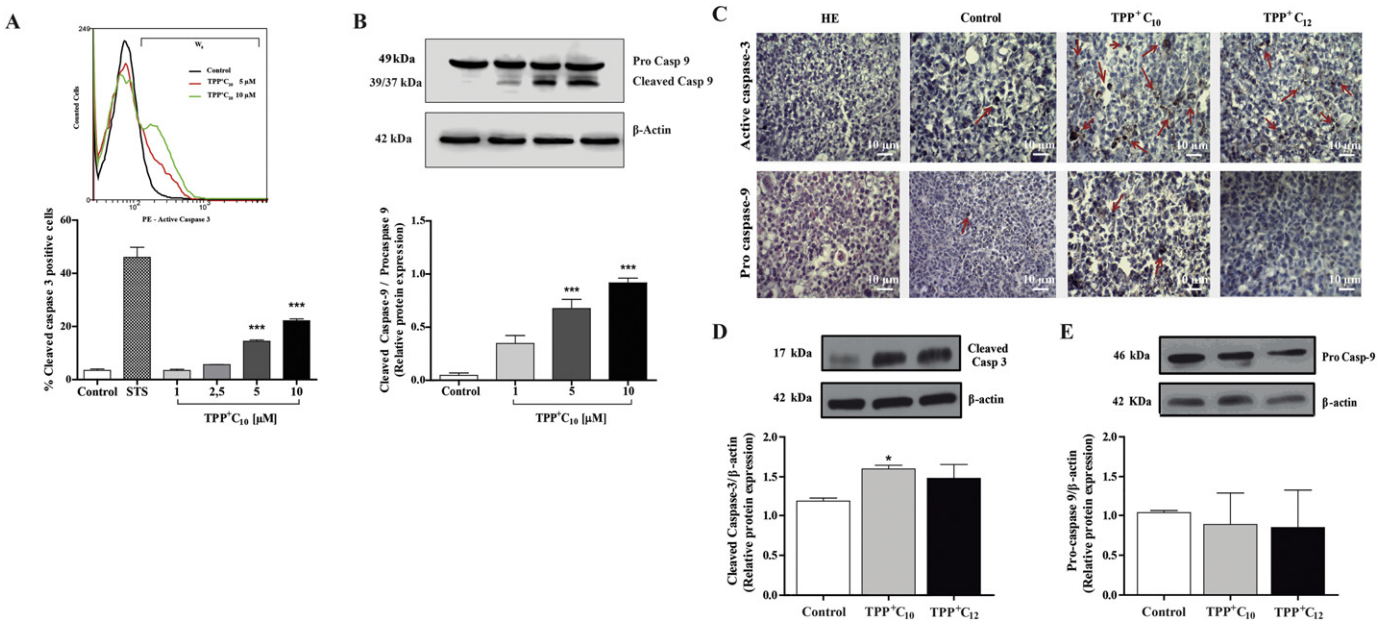

Fig. 5. Effect of TPP^+C_{10} and TPP^+C_{12} on the expression caspase-3 and caspase-9 in TA3/Ha cells and tumor tissue. TA3/Ha cells were treated with increasing concentrations of TPP^+C_{10} as described in the Methods: A. Percentage of cleaved caspase-3 positive cells from three independent experiments. Representative histograms of flow cytometry for cleaved caspase-3. B. Western blotting for active caspase-9 from four independent experiments. One-way ANOVA followed by the Bonferroni post-test. ***$p < 0.001$ indicates a statistically significant difference compared with the control group. Mice were treated with 10 mg/kg body weight of each compound or vehicle as appropriate every 48 h for a period of 30 days: C. Representative immunohistochemical images of active caspase-3 and procaspase-9 expression (three independent experiments) D. Western blot analysis of Cleaved caspase-3 and E. procaspase-9 in tumor tissue. One-way ANOVA followed by the Bonferroni post-test for Western blot analysis. *$p < 0.05$ indicate statistically significant difference compared to the control group. HE: hematoxylin and eosin. Arrows indicate positive labeling. Scale bar: 10 µm.

anabolic reactions as well as the generation of energy and other processes. However, it appears that the degree of dependence on ATP generation *via* OXPHOS or aerobic glycolysis is highly variable depending on the tumor type.

Analysis of oxygen consumption and H^+ release into the extracellular medium enables metabolic characterization of tumor cells. There are three main mechanisms of H^+ release into extracellular medium: 1) release of lactic acid (a product of excretion and an indicator of glycolytic activity) through the monocarboxylate transporter (MCT); 2) activity of extracellular carbonic anhydrase; and 3) activity of Na^+/H^+ exchanger-1 (NHE1) (Molls et al., 2009). Although the last two activities only slightly contribute to H^+ release, they tend to remain constant despite changes in the extracellular medium. Thus, lactate release represents the greatest relevant difference between distinct tumor cell types. Therefore, changes in the glycolytic system can be reflected by changes in acidification of the medium. Oxygen consumption primarily occurs *via* cytochrome *c* oxidase activity (>90%) and generation of reactive oxygen species (>4%). Given the conditions used in the experiment presented in Fig. 1, the main factor contributing to oxygen consumption is electron flow through the mitochondrial respiratory chain.

The substrate glutamine enters the Krebs cycle in the form of α-ketoglutarate. Through enzymatic activities, α-ketoglutarate is transformed into malate and then into oxaloacetate. *Via* anaplerotic reactions, malate and oxaloacetate are transformed into pyruvate, which is transformed into Acetyl-CoA by the enzyme pyruvate dehydrogenase, thus strongly increasing the activity of OXPHOS, as reflected by the significant increase in the respiration rate (Fig. 1B). After 15 min, the respiration rate decreased by 30%, probably due to a high level of mitochondrial OXPHOS-synthesized ATP, which allosterically inhibits cytochrome *c* oxidase activity (Kadenbach et al., 2010). Comparing the results shown in Fig. 1A with those in Fig. 1B, a slight increase in glycolytic flux was noted, probably because some pyruvate was converted to lactate and excreted through MCT, as once the oxygen was fully consumed (anaerobiosis), H^+ release into the environment increased. When only glucose was added (Fig. 1C), the rate of oxygen consumption decreased by 22%, remaining constant until anaerobiosis. This result is consistent with the Crabtree effect of glucose (Diaz-Ruiz et al., 2011). Simultaneously, the H^+ release rate increased by approximately 3.5-fold and remained constant after reaching anaerobiosis (compared with the conditions in Fig. 1B), indicating the large

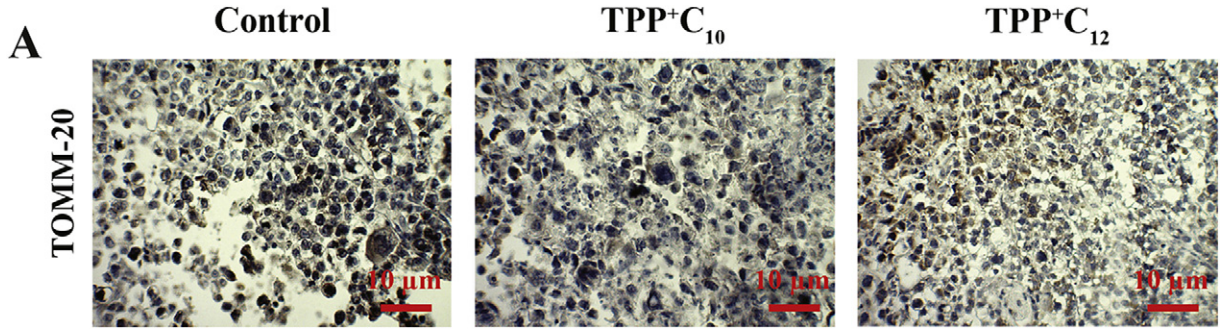

Fig. 6. Effect of TPP^+C_{10} and TPP^+C_{12} on the expression of TOMM-20 in tumor tissue. Mice were treated with 10 mg/kg body weight of each compound or vehicle as appropriate every 48 h for a period of 30 days. A. Representative immunohistochemical images of TOMM-20 from at least two independent experiments. Scale bar: 10 µm.

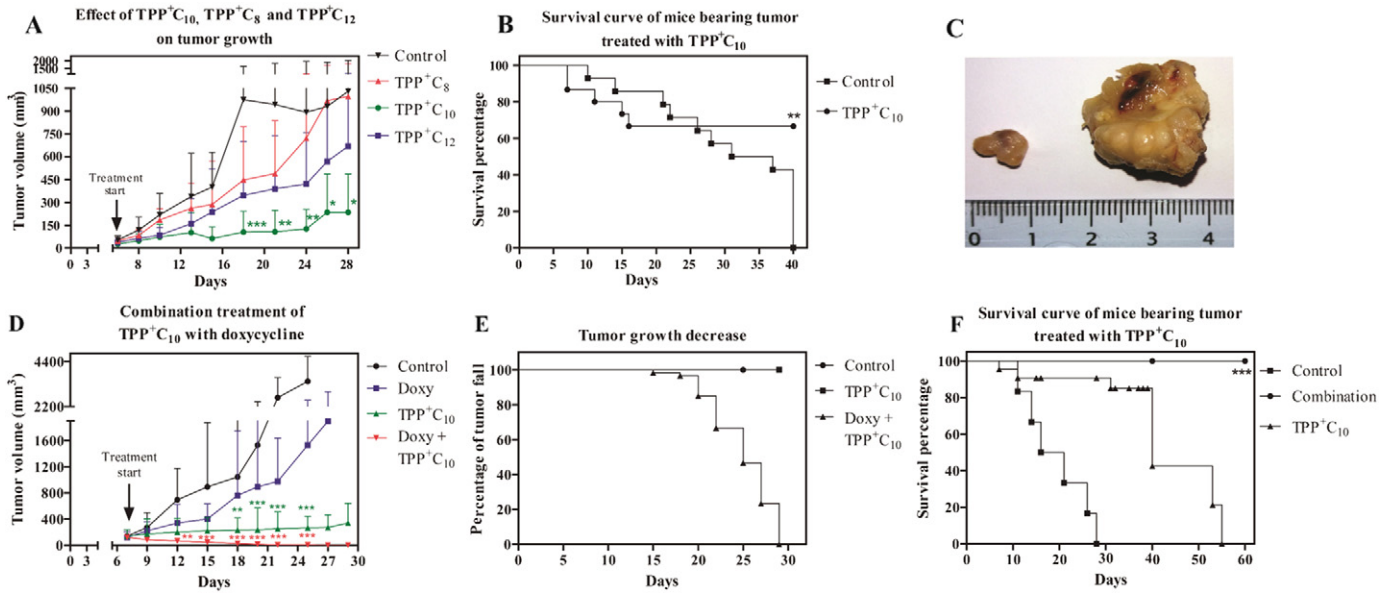

Fig. 7. Effects of alkyl gallate triphenylphosphonium derivatives and the combination of TPP^+C_{10} and doxycycline on tumor growth. For each compound, animals were treated i.p. every 48 h for 28 days as indicated in the methods. The tumor size was measured every 48 h using an external caliper. A. The graph shows the average tumor volume (mm^3) of three independent experiments ($n = 6$ mice per group) for the groups of animals treated with TPP^+C_8, TPP^+C_{10} or TPP^+C_{12}. B. Kaplan-Meier survival curve up to 40 days post-inoculation of tumor-bearing mice treated with 10 mg/kg body weight TPP^+C_{10} ($n = 6$ mice per group for each independent experiment) C. Representative image of a control tumor-bearing mouse in comparison with TPP^+C_{10}-treated tumor-bearing mouse. D. The graph shows the average tumor volume (mm^3) from three independent experiments ($n = 6$ mice per group for each independent experiment) using animals treated with TPP^+C_{10} and/or doxycycline. E. The graph shows the percentage of tumor eradication for each treatment. F. Kaplan Meier survival curve 60 days post-treatment ($n = 6$ mice per group for each independent experiment). Error bars correspond to 95% CI. Two-way ANOVA followed by the Bonferroni post-test. $^*p < 0.05$, $^{**}p < 0.01$, and $^{***}p < 0.001$ indicate statistically significant differences compared to the control group.

contribution of OXPHOS to energy production together with high glycolytic activity in TA3/Ha cells.

When both substrates were added (Fig. 1D), the oxygen consumption rate was similar to that obtained with only glutamine. Nevertheless, the H^+ release rate exhibited two phases, a normoxic phase in which the H^+ release rate was approximately 3.2 times slower than that obtained with only glucose, and another phase that corresponds to the maximal glycolytic flux due to the conditions described. Application of rotenone and Antimycin A caused approximately 90% inhibition of respiration (Fig. 1E–F), provoking drastic stimulation of glycolytic flux. These results indicate that the increase in oxygen consumption is due to ATP synthesis. Interestingly, addition of an inhibitor of ATP synthase (oligomycin) caused the expected decrease in the oxygen consumption rate and increase in glycolytic activity, but addition of the uncoupler CCCP triggered a sharp rise in the oxygen consumption rate and induced a decrease in H^+ release, even under anaerobic conditions. This effect was due to the protonophore activity of CCCP, which caused a loss of $\Delta\Psi_m$, increasing the ATPase activity of ATP synthase (Lou et al., 2007) and repressing the incorporation of Ca^{++} into mitochondria through the mitochondrial calcium uniporter (Santo-Domingo and Demaurex, 2010). These phenomena tend to very quickly decrease the level of intramitochondrial ATP previously synthesized under aerobic conditions, strongly diminishing the enzymatic activity of HK-II. There are many compensatory mechanisms for maintaining ATP levels, including the activity of the intramembrane space enzyme adenylate kinase, which only partially maintains ATP levels. Moreover, mitochondrial uncoupling also produces an important decrease in the level of NAD(P)H (in the presence of oxygen), first within mitochondria and then rapidly extending within the cell (Jara et al., 2014). NADH is necessary for the enzyme lactate dehydrogenase to reduce pyruvate into lactate, which is trapped within the cell. Therefore, we assume that mitochondrial uncoupling induces a rapid increase in oxygen consumption as well as a decrease in acidification of the extracellular medium as a result of decreased glycolytic activity. A similar effect was observed for TTP^+C_{10}, considered a safer uncoupler than CCCP because its effect increases slightly in a broad concentration-dependent manner, extending the range of concentrations between the therapeutic and toxic doses (Jara et al., 2014). Finally, even though OXPHOS is inhibited by oligomycin, when the glycolytic pathway was inhibited by IIA (an inhibitor of G3PDH activity), there was a strong decrease in the release of lactate (Fig. 1I), which would demonstrate that the observed changes in extracellular acidification are largely due to the increased release of lactate *via* glycolytic activity. The metabolic analysis results demonstrated the relationship and dependency between OXPHOS and glycolysis in TA3/Ha cells and provide additional support to the notion that mitochondria are an important therapeutic target in the treatment of cancer.

Several tumor cell lines, including both murine and human cell lines, show broad participation of OXPHOS in the synthesis of total ATP. It has been estimated that the contribution of OXPHOS to total ATP synthesis is nearly 79% in HeLa tumor cells (Rodriguez-Enriquez et al., 2010). Zu and Guppy (2004) established that in a variety of cancer cells, OXPHOS is the main source of ATP despite their increased glycolytic flux. Nevertheless, there is a close relationship between reliance on glycolysis and tumor aggressiveness (Vlassenko et al., 2015).

Treatment with TPP^+C_{10} led to a massive increase in AMP levels and an increase in the ADP/ATP ratio in a concentration-dependent manner (Fig. 2B–C), indicating that TPP^+C_{10} is capable of inducing AMP accumulation at the expense of ADP (adenylate kinase activity) in mitochondria in order to cushion the drastic decrease in total ATP. This finding suggests an important alteration in cellular bioenergetics and an important factor that triggers cell death.

Together with previous findings in our laboratory demonstrating that these derivatives selectively target cancer cells, triggering a decrease in $\Delta\Psi_m$ resulted in reduced ATP levels. Considering these *in vitro* results we established these derivatives as an attractive alternative therapies for fighting cancer in a preclinical model.

The binding of TPP^+ to alkyl gallates directs these molecules to the mitochondria of tumor cells in a highly preferential manner (Fig. 2A). This mechanism has been widely studied (Ganapathy-Kanniappan, 2016), including in the field of therapeutics, as molecules presenting delocalized lipophilic cations are used as tumor markers (Li et al.,

2009). Additionally, the safety of pharmacophores united to TPP^+ has been extensively studied *in vivo*. This is the case for MitoQ and MitoVitE (McManus et al., 2011; Cheng et al., 2013), in which ubiquinol and vitamin E, respectively, were conjugated to TPP^+ to be used as mitochondrial antioxidants in those with cardiovascular and neurodegenerative diseases. MitoQ has been shown to be fairly safe in both animals and humans (Smith and Murphy, 2010). These cationic antioxidant studies not only demonstrated the safety of these compounds but also verified that molecules of high molecular weight attached to delocalized lipophilic cations are able to reach their target site after being administrated systemically. Based on evaluations of body weight changes, damage to specific tissues (Supplementary Figs. 3 and 4), and hematological and biochemical parameters (Table 1), we found that alkyl gallate TPP^+ derivatives do not produce systemic toxicity at doses of 10 mg/kg. This is an important result, as chemotherapy regimens used clinically for breast cancer produce severe adverse effects, which is one of the main obstacles to treatment adhesion (Aiello Bowles et al., 2012; Servitja et al., 2015). Therefore, given this background, alkyl gallate TPP^+ derivatives are a potential alternative to antineoplastic therapy.

Locatelli's group (Locatelli et al., 2012) showed that tetradecyl-gallate reduced tumor growth and metastasis development in an animal model of melanoma *via* induction of NF-κB activity without producing toxicity when administered every three days at 3.7 mg/kg for 28 days. Millard et al. (2010) identified three small molecules bound to TPP^+ (TP187, TP197 and TP421) showing potential antitumor activity without apparent toxicity in a xenograft model. The mechanism proposed was a decrease in oxygen consumption and an increase in superoxide production that subsequently led to cancer cell death. The proposed mechanisms are different from those established in our study, in which increased mitochondrial oxygen consumption and decreased ATP levels were observed.

In infectious disease, antibiotics such as doxycycline (a tetracycline class antibiotic) have well-known metabolic "side effects" on human cells due to mitochondrial disruption. The repurposing of antibiotics may be a novel strategy for the treatment of cancer. Along these lines, doxycycline prevented tumor-sphere formation in 12 cell lines across eight cancer types. In preclinical xenograft models, doxycycline can prevent tumor development and metastasis. Furthermore, clinical trials of antibiotics used to target cancer-associated infections (non-cancer cells) have provided evidence of their antitumor potential. Therefore, we evaluated the ability of doxycycline in combination with TPP^+C_{10} to inhibit mitochondrial biogenesis in TA3/Ha cells and examined how this deleterious effect on mitochondria can be enhanced. As shown in Fig. 3, the combination of doxycycline with TPP^+C_{10} decreased mitochondrial mass in a dose-dependent manner and produced a compensatory increase in the levels of PGC1-α, which is the master regulator of mitochondrial biogenesis. It has been established that overexpression of PGC1-α can prevent muscle atrophy caused by metabolic stress on the muscle (Cannavino et al., 2014). Further, it has been found that a loss of cellular energy balance, seen as an increase in the AMP/ATP ratio leads to the activation of catabolic pathways that drive mitochondrial biogenesis and function through increased expression of PGC1-α (Jager et al., 2007). This observation explains the increase in the protein expression of this transcription factor induced by the combination of TPP^+C_{10} and doxycycline.

The analysis of antitumor activity showed that alkyl gallate TPP^+ derivatives can inhibit cell proliferation (Fig. 4A–B); TPP^+C_{10} was more active than TPP^+C_{12}. This compound produced a noticeable decrease in the expression of the cell proliferation marker Ki-67 (Fig. 4A) as well as an increase in active caspase-3 both *in vitro* (Fig. 5A) and *in vivo* (Fig. 5C–D). This suggests a mechanism by which effectors of cell proliferation and apoptotic cell death can suppress tumor growth *in vivo*. It should be noted that caspase-9 is activated as an acute response to cell stress, however, different mechanisms have been described that lead to the degradation or inhibition of its activity at short times. It has been reported that high rates of caspase-3 activation and high overall amounts of caspase-3, is able to bind directly to the apoptosome suppressing caspase-9 activity, resulting in destabilization of the active apoptosome complex. (Wurstle et al., 2012). In addition, a decrease in the levels of active caspase-9 has been described due to the action of X-linked inhibitor of apoptosis (XIAP). This enzyme directly inhibits the activity of caspase-9, an also induce its ubiquitination and subsequent degradation by the proteosome (Morizane et al., 2005; Steller, 2008; Allan and Clarke, 2009).

These data suggest that at extended stimulation times, the probability of detecting active detecting active caspase-9 is lower. That is why this active fragment was identified *in vitro* after 6 h of stimulation with TPP^+C_{10} (Fig. 5B), but could not be detected after 30 days of treatment with the compound *in vivo* (Fig. 5E). However, caspase-3 activation can be clearly seen both *in vitro* and *in vivo* (Fig. 5A,D). Also, the apoptotic cell death was corroborated through the TUNEL assay (Supplementary Fig. 5). A large positive response was observed through the TUNEL assay compared with activation of caspase 3 by western blot, possibly due that the first assay does not present a high specificity, since several factors influence it especially when it is carried out in tissues (Newbold et al., 2014), which is why it is advisable to corroborate this data with some caspase activation assay, as it was done in this study. In addition, it must be considered that the intrinsic apoptotic pathway is regulated by several caspases and their trigger activation in an amplified response (Elmore, 2007). Due to a significant activation of caspase 3, and a positive response over 80% in TUNEL assay, it is suggested that treatment with TPP^+C_{10} induces an apoptotic cell death. Moreover, treatment with 10 mg/kg TPP^+C_{10} induced a decrease in the levels of TOMM-20 (Fig. 6), a component of the protein complex responsible for the recognition and translocation of mitochondrial protein precursors generated in the cytosol. This protein has been widely used in mass distribution and mitochondrial biogenesis measurements (Whitaker-Menezes et al., 2011), and its expression is associated with mitochondrial content and, therefore, OXPHOS activity (Sotgia et al., 2012). Together, these results suggest that TPP^+C_{10} induces greater mitochondrial activity than the other derivatives *in vivo*. Importantly, these results are related to and complement the results obtained previously *in vitro* (Jara et al., 2014), in which it was established that the mitochondrial uncoupling activity of this compound leads to cytotoxicity and tumor cell death. Most importantly, the molecules GA and triphenylphosphine alone did not induce any changes in tumor growth (Supplementary Fig. 6A–B), indicating that the antitumor activity of these derivatives is due to the complete molecular structure and not its separate components.

Currently, cancer treatment can include the combined use of antineoplastic agents, as administration of drugs with different mechanisms of action is more effective and achieves a better clinical outcome of breast cancer. Consequently, a new drug was incorporated into this study. According to the evidence of its widespread clinical use and safety, the antibiotic doxycycline was chosen to complement the effect of TPP^+C_{10} on tumor growth inhibition in the syngeneic model.

The antitumor activity of doxycycline in different cancer cell lines (Foroodi et al., 2009; Chang et al., 2014; Meng et al., 2014) has been extensively studied, and the findings suggest that doxycycline possesses different mechanisms of action, including inhibition of matrix metalloproteinases and inhibition of mitochondrial biogenesis by tumor cells *via* the inhibition of mitochondrial protein synthesis due to the homology of the 30S bacterial ribosomal subunit to the 28S mitochondrial ribosomal subunit, thus inhibiting mitochondrial function. As a result, combination treatment of TPP^+C_{10} (10 mg/kg/48 h) with doxycycline (10 mg/kg/day) administered i.p. completely eradicated the primary tumor after 30 days (Fig. 7A) without any relapses at 60 days post-treatment. Significantly, neither doxycycline nor TPP^+C_{10} alone completely eliminated the tumor burden. This important finding may be due to a synergistic effect, which can be explained by the use of two compounds with different mechanisms of action: 1) mitochondrial uncoupling induced by TPP^+C_{10}, which triggers metabolic stress due to a drastic

reduction in ATP and a forceful increase in the levels of cytosolic Ca^{++}, accompanied by the release of pro-apoptotic factors, and 2) inhibition of mitochondrial protein elongation and biogenesis by doxycycline. Simultaneously employing these two sets of cytotoxic activities completely eradicated the tumor burden.

The study presented in this work is the first approximation in an animal model with a murine cancer cell line showing the antitumor activity of innovative compounds such as TPP^+C_{10}. Furthermore, the results obtained in the present preclinical study allow us to establish a solid base to extrapolate the research to different models. We have recently demonstrated the effect of these derivatives on an *in vitro* model of human breast cancer, a study focused on the metabolic and mitochondrial alterations triggered by TPP^+ compounds (Sandoval-Acuna et al., 2016), prior to a study in a xenograft murine model. In the same way we have been extending our research to other cancers of high prevalence.

5. Conclusions

In this study, we have shown the therapeutic antitumor potential of alkyl gallate TPP^+ derivatives. We established that the TPP^+ moiety is an important tool for guiding a pharmacophore, selectively targeting the mitochondria of cancer cells, and, most importantly, achieving selectivity to mitochondria of tumor cells in an animal model without producing systemic toxicity. It was established that among the GA derivatives tested, the compound that contained a saturated chain of ten carbon atoms (TPP^+C_{10}) showed greater inhibition of tumor growth. Moreover, administering TPP^+C_{10} in combination with doxycycline completely eradicated the tumor burden. Given these results, it is important to further study animal models of cancer produced using human cells to establish whether this treatment is a valuable candidate strategy for the fight against breast cancer.

Author contributions

L.P-S., S·F-R., and J.F. designed the study. M.M-R., S.R and V·C-C synthesized the compounds. L.P-S., S.F-R., and M.P. performed the experimental work. L.P-S., S.F-R., C.S-A, U.K. and J.F. analyzed and interpreted the data. L.P-S., S.F-R., and J.F. wrote the manuscript. J.D.M., U.K. and E.P. provided valuable administrative, technical and material support.

Notes

The authors declare no competing financial interest.

Acknowledgments

This work was supported by the following grants: FONDECYT 1130772 and VID ENL022/16 (J. Ferreira), ERANET-LAC ELAC2014/HID328 (U. Kemmerling) and CONICYT Ph.D. fellowship 21110084 (L. Peredo-Silva).

Appendix A. Supplementary data

Supplementary data to this article can be found online at http://dx.doi.org/10.1016/j.taap.2017.06.017.

References

Aiello Bowles, E.J., Boudreau, D.M., Chubak, J., Yu, O., Fujii, M., Chestnut, J., Buist, D.S., 2012. Patient-reported discontinuation of endocrine therapy and related adverse effects among women with early-stage breast cancer. J. Oncol. Pract. 8, e149–e157.

Allan, L.A., Clarke, P.R., 2009. Apoptosis and autophagy: regulation of caspase-9 by phosphorylation. FEBS J. 276, 6063–6073.

Cannavino, J., Brocca, L., Sandri, M., Bottinelli, R., Pellegrino, M.A., 2014. PGC1-alpha overexpression prevents metabolic alterations and soleus muscle atrophy in hindlimb unloaded mice. J. Physiol. 592, 4575–4589.

Chang, M.Y., Rhee, Y.H., Yi, S.H., Lee, S.J., Kim, R.K., Kim, H., Park, C.H., Lee, S.H., 2014. Doxycycline enhances survival and self-renewal of human pluripotent stem cells. Stem Cell Rep. 3, 353–364.

Cheng, G., Zielonka, J., McAllister, D.M., Mackinnon, A.C., Joseph, J., Dwinell, M.B., Kalyanaraman, B., 2013. Mitochondria-targeted vitamin E analogs inhibit breast cancer cell energy metabolism and promote cell death. BMC Cancer 13, 285.

Coulter, C.V., Kelso, G.F., Lin, T.K., Smith, R.A., Murphy, M.P., 2000. Mitochondrially targeted antioxidants and thiol reagents. Free Radic. Biol. Med. 28, 1547–1554.

Diaz-Ruiz, R., Rigoulet, M., Devin, A., 2011. The Warburg and Crabtree effects: on the origin of cancer cell energy metabolism and of yeast glucose repression. Biochim. Biophys. Acta 1807, 568–576.

Duivenvoorden, W.C., Popović, S.V., Lhoták, S., Seidlitz, E., Hirte, H.W., Tozer, R.G., Singh, G., 2002. Doxycycline decreases tumor burden in a bone metastasis model of human breast cancer. Cancer Res. 62, 1588–1591.

Elmore, S., 2007. Apoptosis: a review of programmed cell death. Toxicol. Pathol. 35, 495–516.

Fiuza, S.M., Gomes, C., Teixeira, L.J., Girao da Cruz, M.T., Cordeiro, M.N., Milhazes, N., Borges, F., Marques, M.P., 2004. Phenolic acid derivatives with potential anticancer properties—a structure-activity relationship study. Part 1: methyl, propyl and octyl esters of caffeic and gallic acids. Bioorg. Med. Chem. 12, 3581–3589.

Foroodi, F., Duivenvoorden, W.C., Singh, G., 2009. Interactions of doxycycline with chemotherapeutic agents in human breast adenocarcinoma MDA-MB-231 cells. Anti-Cancer Drugs 20, 115–122.

Ganapathy-Kanniappan, S., 2016. Targeting tumor glycolysis by a mitotropic agent. Expert Opin. Ther. Targets 20, 1–5.

Han, D.W., Matsumura, K., Kim, B., Hyon, S.H., 2008. Time-dependent intracellular trafficking of FITC-conjugated epigallocatechin-3-O-gallate in L-929 cells. Bioorg. Med. Chem. 16, 9652–9659.

van der Heijden, C.A., Janssen, P.J., Strik, J.J., 1986. Toxicology of gallates: a review and evaluation. Food Chem. Toxicol. 24, 1067–1070.

Jager, S., Handschin, C., St-Pierre, J., Spiegelman, B.M., 2007. AMP-activated protein kinase (AMPK) action in skeletal muscle via direct phosphorylation of PGC-1alpha. Proc. Natl. Acad. Sci. U. S. A. 104, 12017–12022.

Jara, J.A., Castro-Castillo, V., Saavedra-Olavarria, J., Peredo, L., Pavanni, M., Jana, F., Letelier, M.E., Parra, E., Becker, M.I., Morello, A., Kemmerling, U., Maya, J.D., Ferreira, J., 2014. Antiproliferative and uncoupling effects of delocalized, lipophilic, cationic gallic acid derivatives on cancer cell lines. Validation in vivo in singenic mice. J. Med. Chem. 57, 2440–2454.

Ji, B.C., Hsu, W.H., Yang, J.S., Hsia, T.C., Lu, C.C., Chiang, J.H., Yang, J.L., Lin, C.H., Lin, J.J., Suen, L.J., Gibson Wood, W., Chung, J.G., 2009. Gallic acid induces apoptosis via caspase-3 and mitochondrion-dependent pathways in vitro and suppresses lung xenograft tumor growth in vivo. J. Agric. Food Chem. 57, 7596–7604.

Kadenbach, B., Ramzan, R., Wen, L., Vogt, S., 2010. New extension of the Mitchell theory for oxidative phosphorylation in mitochondria of living organisms. Biochim. Biophys. Acta 1800, 205–212.

Kang, M.S., Oh, J.S., Kang, I.C., Hong, S.J., Choi, C.H., 2008. Inhibitory effect of methyl gallate and gallic acid on oral bacteria. J. Microbiol. 46, 744–750.

Kim, Y.S., Yang, C.T., Wang, J., Wang, L., Li, Z.B., Chen, X., Liu, S., 2008. Effects of targeting moiety, linker, bifunctional chelator, and molecular charge on biological properties of 64Cu-labeled triphenylphosphonium cations. J. Med. Chem. 51, 2971–2984.

Kratz, J.M., Andrighetti-Fröhner, C.R., Leal, P.C., Nunes, R.J., Yunes, R.A., Trybala, E., Bergström, T., Barardi, C.R., Simões, C.M., 2008. Evaluation of anti-HSV-2 activity of gallic acid and pentyl gallate. Biol. Pharm. Bull. 31, 903–907.

Lamb, R., Ozsvari, B., Lisanti, C.L., Tanowitz, H.B., Howell, A., Martinez-Outschoorn, U.E., Sotgia, F., Lisanti, M.P., 2015. Antibiotics that target mitochondria effectively eradicate cancer stem cells, across multiple tumor types: treating cancer like an infectious disease. Oncotarget 6, 4569–4584.

Li, Z., Lopez, M., Hardy, M., McAllister, D.M., Kalyanaraman, B., Zhao, M., 2009. A 99mTc-labeled triphenylphosphonium derivative for the early detection of breast tumors. Cancer Biother. Radiopharm. 24, 579–587.

Locatelli, C., Rosso, R., Santos-Silva, M.C., de Souza, C.A., Licinio, M.A., Leal, P., Bazzo, M.L., Yunes, R.A., Creczynski-Pasa, T.B., 2008. Ester derivatives of gallic acid with potential toxicity toward L1210 leukemia cells. Bioorg. Med. Chem. 16, 3791–3799.

Locatelli, C., Leal, P.C., Yunes, R.A., Nunes, R.J., Creczynski-Pasa, T.B., 2009. Gallic acid ester derivatives induce apoptosis and cell adhesion inhibition in melanoma cells: the relationship between free radical generation, glutathione depletion and cell death. Chem. Biol. Interact. 181, 175–184.

Locatelli, C., Carvalho, D.R., Mascarello, A., de Cordova, C.A., Yunes, R.A., Nunes, R.J., Pilati, C., Creczynski-Pasa, T.B., 2012. Antimetastatic activity and low systemic toxicity of tetradecyl gallate in a preclinical melanoma mouse model. Investig. New Drugs 30, 870–879.

Lopez-Rios, F., Sanchez-Arago, M., Garcia-Garcia, E., Ortega, A.D., Berrendero, J.R., Pozo-Rodriguez, F., Lopez-Encuentra, A., Ballestin, C., Cuezva, J.M., 2007. Loss of the mitochondrial bioenergetic capacity underlies the glucose avidity of carcinomas. Cancer Res. 67, 9013–9017.

Losada Barreiro, S., Bravo-Diaz, C., Paiva-Martins, F., Romsted, L.S., 2013. Maxima in antioxidant distributions and efficiencies with increasing hydrophobicity of gallic acid and its alkyl esters. The pseudophase model interpretation of the "cutoff effect". J. Agric. Food Chem. 61, 6533–6543.

Lou, P.H., Hansen, B.S., Olsen, P.H., Tullin, S., Murphy, M.P., Brand, M.D., 2007. Mitochondrial uncouplers with an extraordinary dynamic range. Biochem. J. 407, 129–140.

Lu, Z., Nie, G., Belton, P.S., Tang, H., Zhao, B., 2006. Structure-activity relationship analysis of antioxidant ability and neuroprotective effect of gallic acid derivatives. Neurochem. Int. 48, 263–274.

Maurya, D.K., Nandakumar, N., Devasagayam, T.P.A., 2011. Anticancer property of gallic acid in A549, a human lung adenocarcinoma cell line, and possible mechanisms. J. Clin. Biochem. Nutr. 48, 85–90.
McManus, M.J., Murphy, M.P., Franklin, J.L., 2011. The mitochondria-targeted antioxidant MitoQ prevents loss of spatial memory retention and early neuropathology in a transgenic mouse model of Alzheimer's disease. J. Neurosci. 31, 15703–15715.
Meng, J., Sun, B., Zhao, X., Zhang, D., Zhao, X., Gu, Q., Dong, X., Zhao, N., Liu, P., Liu, Y., 2014. Doxycycline as an inhibitor of the epithelial-to-mesenchymal transition and vasculogenic mimicry in hepatocellular carcinoma. Mol. Cancer Ther. 13, 3107–3122.
Millard, M., Pathania, D., Shabaik, Y., Taheri, L., Deng, J., Neamati, N., 2010. Preclinical evaluation of novel triphenylphosphonium salts with broad-spectrum activity. PLoS One 5, e13131.
Modica-Napolitano, J.S., Singh, K.K., 2004. Mitochondrial dysfunction in cancer. Mitochondrion 4, 755–762.
Molls, M., Vaupel, P., Nieder, C., Anscher, M.S., 2009. In: Baert, A.L., Brady, L.W., Heilmann, H.P., Knauth, M., Molls, M., Nieder, C. (Eds.), The impact of tumor biology on cancer treatment and multidisciplinary strategies. Springer, Germany, pp. 76–79.
Morizane, Y., Honda, R., Fukami, K., Yasuda, H., 2005. X-linked inhibitor of apoptosis functions as ubiquitin ligase toward mature caspase-9 and cytosolic Smac/DIABLO. J. Biochem. 137, 125–132.
Murphy, M.P., Smith, R.A., 2007. Targeting antioxidants to mitochondria by conjugation to lipophilic cations. Annu. Rev. Pharmacol. Toxicol. 47, 629–656.
Newbold, A., Martin, B.P., Cullinane, C., Bots, M., 2014. Detection of apoptotic cells using immunohistochemistry. Cold Spring Harb Protoc 2014, 1196–1201.
Pedersen, P.L., 2007. The cancer cell's "power plants" as promising therapeutic targets: an overview. J. Bioenerg. Biomembr. 39, 1–12.
Putignani, L., Raffa, S., Pescosolido, R., Aimati, L., Signore, F., Torrisi, M.R., Grammatico, P., 2008. Alteration of expression levels of the oxidative phosphorylation system (OXPHOS) in breast cancer cell mitochondria. Breast Cancer Res. Treat. 110, 439–452.
Rodriguez-Enriquez, S., Carreno-Fuentes, L., Gallardo-Perez, J.C., Saavedra, E., Quezada, H., Vega, A., Marin-Hernandez, A., Olin-Sandoval, V., Torres-Marquez, M.E., Moreno-Sanchez, R., 2010. Oxidative phosphorylation is impaired by prolonged hypoxia in breast and possibly in cervix carcinoma. Int. J. Biochem. Cell Biol. 42, 1744–1751.
Rosano, C., 2011. Molecular model of hexokinase binding to the outer mitochondrial membrane porin (VDAC1): implication for the design of new cancer therapies. Mitochondrion 11, 513–519.
Sandoval-Acuna, C., Fuentes-Retamal, S., Guzman-Rivera, D., Peredo-Silva, L., Madrid-Rojas, M., Rebolledo, S., Castro-Castillo, V., Pavani, M., Catalan, M., Maya, J.D., Jara, J.A., Parra, E., Calaf, G.M., Speisky, H., Ferreira, J., 2016. Destabilization of mitochondrial functions as a target against breast cancer progression: role of TPP(+)-linked-polyhydroxybenzoates. Toxicol. Appl. Pharmacol. 309, 2–14.
Santo-Domingo, J., Demaurex, N., 2010. Calcium uptake mechanisms of mitochondria. Biochim. Biophys. Acta 1797, 907–912.
Servitja, S., Martos, T., Rodriguez Sanz, M., Garcia-Giralt, N., Prieto-Alhambra, D., Garrigos, L., Nogues, X., Tusquets, I., 2015. Skeletal adverse effects with aromatase inhibitors in early breast cancer: evidence to date and clinical guidance. Ther. Adv. Med. Oncol. 7, 291–296.
Shen, L.C., Chen, Y.K., Lin, L.M., Shaw, S.Y., 2010. Anti-invasion and anti-tumor growth effect of doxycycline treatment for human oral squamous-cell carcinoma—in vitro and in vivo studies. Oral Oncol. 46, 178–184.
Smith, R.A., Murphy, M.P., 2010. Animal and human studies with the mitochondria-targeted antioxidant MitoQ. Ann. N. Y. Acad. Sci. 1201, 96–103.
Sotgia, F., Whitaker-Menezes, D., Martinez-Outschoorn, U.E., Flomenberg, N., Birbe, R.C., Witkiewicz, A.K., Howell, A., Philp, N.J., Pestell, R.G., Lisanti, M.P., 2012. Mitochondrial metabolism in cancer metastasis: visualizing tumor cell mitochondria and the "reverse Warburg effect" in positive lymph node tissue. Cell Cycle 11, 1445–1454.
Spill, F., Reynolds, D.S., Kamm, R.D., Zaman, M.H., 2016. Impact of the physical microenvironment on tumor progression and metastasis. Curr. Opin. Biotechnol. 40, 41–48.
Steller, H., 2008. Staying alive: apoptosome feedback inhibition. Nat. Cell Biol. 10, 1387–1388.
Verma, S., Singh, A., Mishra, A., 2013. Gallic acid: molecular rival of cancer. Environ. Toxicol. Pharmacol. 35, 473–485.
Vlassenko, A.G., McConathy, J., Couture, L.E., Su, Y., Massoumzadeh, P., Leeds, H.S., Chicoine, M.R., Tran, D.D., Huang, J., Dahiya, S., Marcus, D.S., Fouke, S.J., Rich, K.M., Raichle, M.E., Benzinger, T.L., 2015. Aerobic glycolysis as a marker of tumor aggressiveness: preliminary data in high grade human brain tumors. Dis. Markers 2015, 874904.
Whitaker-Menezes, D., Martinez-Outschoorn, U.E., Flomenberg, N., Birbe, R.C., Witkiewicz, A.K., Howell, A., Pavlides, S., Tsirigos, A., Ertel, A., Pestell, R.G., Broda, P., Minetti, C., Lisanti, M.P., Sotgia, F., 2011. Hyperactivation of oxidative mitochondrial metabolism in epithelial cancer cells in situ: visualizing the therapeutic effects of metformin in tumor tissue. Cell Cycle 10, 4047–4064.
Wurstle, M.L., Laussmann, M.A., Rehm, M., 2012. The central role of initiator caspase-9 in apoptosis signal transduction and the regulation of its activation and activity on the apoptosome. Exp. Cell Res. 318, 1213–1220.
Yeh, R.D., Chen, J.C., Lai, T.Y., Yang, J.S., Yu, C.S., Chiang, J.H., Lu, C.C., Yang, S.T., Yu, C.C., Chang, S.J., Lin, H.Y., Chung, J.G., 2011. Gallic acid induces G_0/G_1 phase arrest and apoptosis in human leukemia HL-60 cells through inhibiting cyclin D and E, and activating mitochondria-dependent pathway. Anticancer Res. 31, 2821–2832.
Yoon, C.H., Chung, S.J., Lee, S.W., Park, Y.B., Lee, S.K., Park, M.C., 2013. Gallic acid, a natural polyphenolic acid, induces apoptosis and inhibits proinflammatory gene expressions in rheumatoid arthritis fibroblast-like synoviocytes. Joint, bone, spine. Rev. Rhum. 80, 274–279.
Zu, X.L., Guppy, M., 2004. Cancer metabolism: facts, fantasy, and fiction. Biochem. Biophys. Res. Commun. 313, 459–465.